CREATION OF A REMOTE SENSING UNMANNED AERIAL SYSTEM (UAS) FOR PRECISION AGRICULTURE AND RELATED MAPPING APPLICATIONS

Dimitrios Stefanakis
John N. Hatzopoulos
Nikolaos Margaris
University of Aegean, Department of the Environment
Nikolaos Danalatos
University of Thessaly, Department of Agriculture

PURPOSE

Our goal is to create a fully autonomous airborne remote sensing platform, for the production of various vegetation indices to determine growth, development, yield crop and provide considerable information in real time and at low cost (compared with existing methods) for the study area.

The primary tool for extraction and production of the information is an unmanned aerial system (UAS) that carries sensors and cameras flying over the study area, transmitting real time data that has been programmed to collect. The collected data is land cover, geographic location, weather data, geomorphologic and cadastral data, ortho-corrected derivatives and qualitative data type coverage, biomass and other parameters that have been introduced to the platform via computational GIS routines.

This idea emerged during the analysis of the functional ecology in Greek agro-ecosystems within spatial information and mapping. To take full advantage of dynamic tools of IT, such as Geographic Information Systems and Expert Systems, Global Positioning Systems, Remote Sensing and Agriculture Engineering tools.

The platform named "Skiptrovamon" has numerous applications and is used as a tool in many scientific fields, such as; precision agriculture, geography, geomorphology, topography, urban geography, and remote sensing.

Skiptrovamon was designed and has been tested as remote sensing platform for precision agriculture. As the aircraft flies over the study area it collects information from cropland and outputs, yield crop, current biomass, indicate the stressed plants and possible lack or adequate irrigation and fertilization in real time through computational routines.

Key words: UAS, Skiptrovamon, agriculture, remote sensing, GIS

INTRODUCTION

Background

Computational routines - models are by default simplified expressions of more complex systems and only a fraction of reality (De Wit, 1968, 1993), in any case they cannot represent the full range of a real system. Therefore biological models and crop development models cannot be used in cases other than those for which they were designed for. The purpose of building a model is to simplify as far as possible and study of a particular part of reality that we need for a particular topic under study (Van Laar, 1994). These models began to be known and to assist in resolving and understanding the physiology with the appearance of P/C's, 30 years ago (Duncan et al., 1967; Goudriaan, 1977).

However, crop growth and development simulation, focuses on the hierarchical level of crops potential output (de Wit & Penning de Vries, 1982; D riessen & Konijn, 1992), in which water and nutrients are available to the crop. Therefore soil processes and the development of root zone does not need to be analyzed. Also it does not take into account any reductions in production capacity of weeds and pests. So in this first hierarchical level of

potential output, increasing crop depends only on the processes taking place above ground, such as assimilation, crop growth, respiration and allocation of dry matter to different plant organs. Moving to a lower hierarchical level with our modern computers became possible with sub-models to reach potential output which additionally depends on the availability of water and nutrients (Danalatos et al., 2004).

In any case, existing models and monitoring processes, are focusing their results to the exact point of the study area, giving us a quantitative overview of the variables, without spatial representation, which is closely connected with the agriculture and the environment.

Geographic Information Systems (GIS), in conjunction with the Remote sensing (Hatzopoulos J. N., 2008), made possible to capitalize the plethora of models (Almhab et al., 2008) and for the first time to reverse the outcome of the results from point (focal) level to local level (local) (Xiaopeng et al., 2011) thereby making possible for two-way use and displaying them in space and time. Also we can achieve significantly faster results due to automated supply of our system (GIS & models) from the UAS based on Arduino (Hideki et al., 2008) and continuously feeding with the required data. The ground models can easily be calibrated along with the model machine learning method (Gashler, 2011).

Objectives

The objectives of the research are:

A. Translate, a precision agriculture mathematical model dry weight increase (DWI) to GIS computational routine and take advantage of the Auto-pilots IMU and payload cameras, to collect usable weather and plant data.

In order to make calculation within the collected and given data, we have to transform them to surface models. A surface in the geographical space is a continuous field of values, which differ in value and their spatial position (location), they are called spatial attributes. Considering all the spatial interpolation methods, the Kriging spatial interpolation is based on good theoretical basis, provides a convincing calculation method for interpolated values and is considered as the Best Linear Unbiased Estimator (www.geosciences.mines-paristech.fr). The basic idea is to first discover the characteristics of spatial distribution and then apply these properties to calculate the remaining values of the surface. The relatively accurate prediction of values is the largest capacity and operates with a different statistical approach compared with other interpolation methods. Thus, this method considers the distance and direction between the reflections of sampling points and their spatial correlation, which can be used to explain the changes in the surface. In our case it will be applied to identify and calculate the values of climatic and Plant parameters required as unknowns in our computational routines.

B. Design, construct and develop an airborne platform, capable to perform automated lawnmower patterns and carry all the necessary equipment, required for remote sensing. The platform should have a flight envelop to achieve optimized image captures (cruise airspeed), flight time to capture the mean cultivated property in Mediterranean ~300 acres (current consumption), maneuverability and agility, to overcome the wind gusts and mountainous terrain (max airspeed) and a rigid airframe and components to achieve landing thru cultivated areas.

Furthermore to create a fully autonomous airborne remote sensing platform, for the production of various vegetation indices to determine growth, development, crop yield and provide considerable information in real time and at low cost (compared with existing methods) for the study area.

C. Combine remotely sensed acquired data from our UAS and the existing DWI estimation model, to our GIS system, to calculate the DWI, for corn crop of a Greek county, Larissa.

MATERIALS AND METHODS

Methods

Translating the DWI model to GIS routine. Solar energy converted to biomass by the process of photosynthesis. In this process, the CO_2 of the air is converted into carbohydrate $(CH_2O)n$ according to the generalized reaction:

$CO_2 + H_2O + solar\ energy \rightarrow 1/n\ (CH_2O)n + O_2$ (1)
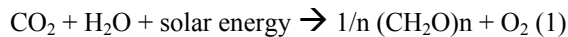
A part of the produced carbohydrates used as structural material of plant mass as for example lignin, protein, fat, etc., while another part is used as an energy source for various functions of the plant:

$1/n\ (CH_2O)n + O_2 \rightarrow CO_2 + H_2O + chemical\ energy$ (2)
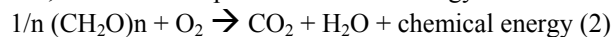
With known latitude and day of the year, the rate of uptake of a closed leaf canopy on a cloudless and a fully overcast day is determined by (linear) interpolation. This rate for partially overcast days can be calculated with the equation:

FGC = FO * FOV + (1 - FO) * FCL (3)

Where,

FGC is the total rate of assimilation leaf canopy (kg ha -1 d -1),

FO is the percentage of days that the sky is cloud (FO = 0 for a completely cloudless day, and FO = 1 for completely overcast days).

FOV is total assimilation rate leaf canopy a completely overcast day (kg ha -1 d -1), and

FCL is total assimilation rate leaf canopy a completely cloudless day (kg ha -1 d -1), (Tables 1.1, 1.2)

The percentage of days that the sky is cloud determined from the (specific) daily solar radiation and that which corresponds to fully cloudless day as shown in Table 1.

Table 1. (A) Total radiation, TOTRAD (10^6 J m -2 d -1) for typical cloudless day. and (b) maximum sunshine duration (h), as a function of latitude and day of year.

Date N. Hemisphere S. Hemisphere	15 Jan Jul	15 Feb Aug	15 Mar Sep	15 Apr Oct	15 May Nov	15 June Dec	15 Jul Jan	15 Aug Feb	15 Sep Mar	15 Oct Apr	15 Nov May	15 Dec Jun
Latitude					(a) TOTRAD (10^6 J m -2 d -1)							
0°	28.00	29.44	30.32	29.90	28.52	27.54	27.94	29.36	30.34	29.88	28.46	27.54
10°	24.34	26.88	29.34	30.86	30.96	30.68	30.82	31.02	30.18	27.90	25.10	23.60
20°	20.00	22.46	27.36	30.76	32.44	32.92	32.76	31.68	28.96	24.98	21.00	19.06
30°	15.18	19.30	24.42	29.62	32.90	34.24	33.74	31.28	26.74	21.34	16.34	14.10
40°	10.12	14.60	20.64	27.48	32.36	34.58	33.72	29.86	23.60	16.80	11.34	9.00
50°	5.22	9.60	16.14	24.40	30.88	34.02	32.82	27.50	19.60	11.92	6.38	4.22
60°	1.22	4.68	11.16	20.50	28.62	32.86	31.20	24.30	14.94	6.84	2.00	0.64
					(b) maximum sunshine duration (h)							
0°	12.1	12.1	12.1	12.1	12.1	12.1	12.1	12.1	12.1	12.1	12.1	12.1
10°	11.7	11.8	12.0	12.4	12.5	12.7	12.7	12.5	12.2	11.9	11.7	11.5
20°	11.1	11.5	12.0	12.6	13.1	13.3	13.2	12.9	12.3	11.7	11.3	11.0
30°	10.4	11.2	11.9	12.9	13.6	14.0	13.9	13.3	12.4	11.5	10.8	10.3
40°	9.9	10.7	11.8	13.3	14.3	14.9	14.7	13.9	12.5	11.2	10.1	9.5
50°	9.2	10.2	11.6	13.8	15.3	16.2	15.9	14.6	12.6	10.9	9.3	8.3
60°	7.5	9.2	11.4	14.6	17.0	18.5	18.0	15.9	12.9	10.3	7.2	6.4

Table 1.1 Calculated assimilation rate values CO_2 (kg ha -1 d -1) for closed leaf canopy with spherical leaf distribution, for cloudless (FCL) and completely overcast (FOV) days, and a maximum photosynthetic rate, AMAX=40 kg ha -1 d -1.

Date N. Hemisphere S. Hemisphere		15 Jan Jul	15 Feb Aug	15 Mar Sept	15 Apr Oct	15 May Nov	15 Jun Dec	15 Jul Jan	15 Aug Feb	15 Sep Mar	15 Oct Apr	15 Nov May	15 Dec Jun
Latitude													
0°	Fcl	728	753	768	761	737	720	727	752	768	760	736	720
	Fov	306	320	328	324	311	302	306	319	328	324	311	302
10°	Fcl	652	701	748	779	786	784	785	784	765	720	667	638
	Fov	270	295	319	334	336	333	335	336	327	305	277	262
20°	Fcl	562	634	713	783	820	834	829	802	745	665	583	542
	Fov	226	261	300	334	351	356	355	343	316	276	236	216
30°	Fcl	454	549	659	768	839	869	858	804	708	591	481	429
	Fov	175	219	271	324	357	371	366	341	295	239	187	163
40°	Fcl	333	445	586	737	843	892	873	788	652	497	364	304
	Fov	120	169	233	304	354	377	368	329	264	193	133	107
50°	Fcl	202	324	491	686	833	904	877	757	574	384	234	172
	Fov	63	114	187	275	343	375	363	307	224	140	77	52
60°	Fcl	68	191	375	615	813	915	875	708	474	255	102	39
	Fov	15	57	132	236	323	368	351	277	175	83	25	8
70°	Fcl	0	46	240	527	798	967	896	649	353	114	0	0
	Fov	0	10	73	189	302	369	341	240	118	27	0	0

(Source: Goudriaan & Van Laar, 1978)

Table 1.2. Calculated assimilation rate values CO_2 (kg ha -1 d -1) for closed leaf canopy with spherical leaf distribution, for cloudless (FCL) and completely overcast (FOV) days, and a maximum photosynthetic rate, AMAX=70 kg ha -1 d -1.

Date N. Hemisphere S. Hemisphere		15 Jan Jul	15 Feb Aug	15 Mar Sept	15 Apr Oct	15 May Nov	15 Jun Dec	15 Jul Jan	15 Aug Feb	15 Sep Mar	15 Oct Apr	15 Nov May	15 Dec Jun
Latitude													
0°	Fcl	959	995	1017	1007	973	947	958	993	1018	1007	971	947
	Fov	326	341	350	346	331	321	325	340	351	346	331	321
10°	Fcl	852	922	989	1032	1039	1035	1037	1038	1012	949	873	832
	Fov	285	313	340	357	358	356	357	359	349	324	294	277
20°	Fcl	726	827	937	1035	1086	1103	1097	1062	983	870	755	698
	Fov	237	276	319	356	375	381	379	366	336	292	248	226
30°	Fcl	577	707	860	1011	1109	1149	1134	1060	927	765	613	542
	Fov	182	229	287	345	381	396	391	363	313	251	195	170
40°	Fcl	410	562	755	962	1108	1175	1150	1033	845	633	452	372
	Fov	123	176	245	322	377	402	392	349	278	201	138	110
50°	Fcl	236	397	620	885	1086	1183	1145	982	733	477	278	198
	Fov	65	117	194	289	362	398	384	324	234	145	78	53
60°	Fcl	71	220	460	779	1046	1182	1129	905	591	301	109	40
	Fov	15	58	136	246	340	388	369	290	181	85	25	8
70°	Fcl	0	47	277	649	1006	1222	1132	810	421	121	0	0
	Fov	0	10	74	195	314	385	356	249	120	28	0	0

(Source: Goudriaan & Van Laar, 1978)

Table 2 Photosynthetic mechanism (C3/C4), specific leaf area (SLA, m2 / kg) penetration rate for the visible spectrum (KE), respiration rate relative retention (RMorg, kg-1d-1), and conversion of dry substance, EC (kg kg-1), for a number of crops.

Crop	C3 / C4	SLA (range)	KE	RM (org)*				EC (org)*			
				RML	RMR	RMS	RMSO	ECL	ECR	ECS	ECSO
Groundnut	C3	18	0.6	0.030	0.010	0.015	0.012	0.72	0.72	0.69	0.50
Cotton	C3	16-24	0.6	0.010	0.010	0.015	0.010	0.72	0.72	0.69	0.61
Sweet potato	C3	14-20	0.45	0.028	0.025	0.020	0.005	0.72	0.72	0.69	0.80
Horsegram	C3	32-40	0.5	0.030	0.010	0.015	0.011	0.72	0.72	0.69	0.81
Sunflower	C3	25-30	0.8	0.015	0.010	0.0075	0.023	0.59	0.71	0.73	0.71
Corn	C4	12-32	0.6	0.013	0.010	0.010	0.010	0.72	0.72	0.69	0.72
Smoke	C3	10-31	0.5	0.015	0.010	0.015	--	0.72	0.72	0.69	--
Barley	C3	18-27	0.44	0.015	0.010	0.015	0.007	0.72	0.72	0.69	0.74
Millet	C3	18-23	0.5	0.020	0.007	0.010	0.007	0.72	0.72	0.69	0.74
Pea	C3	20-28	0.5	0.030	0.010	0.015	0.010	0.72	0.72	0.69	0.78
Potato	C3	25-32	0.5	0.010	0.010	0.015	0.007	0.72	0.72	0.69	0.85
Chickpea	C3	15-20	0.5	0.030	0.010	0.015	0.009	0.72	0.72	0.69	0.77
Rice	C3	18-27	0.4	0.015	0.010	0.015	0.0035	0.72	0.72	0.69	0.74
Wheat	C3	16-24	0.5	0.017	0.010	0.015	0.010	0.72	0.72	0.69	0.79
Soy	C3	15-23	0.4	0.015	0.010	0.015	0.017	0.72	0.72	0.69	0.68
Sorghum	C4	11-21	0.5	0.015	0.010	0.010	0.010	0.72	0.72	0.69	0.74
Sesame	C3	21-30	0.5	0.015	0.010	0.015	0.012	0.72	0.72	0.69	0.62
Lentil	C3	32-37	0.5	0.015	0.010	0.015	0.013	0.72	0.72	0.69	0.71

* org = L (Leaf), R (Root), S (Stem), SO =Storage organs. (Source: Driessen & Konijn, 1992).

The daily global radiation on a fully cloudy day can be determined by multiplying the value for full cloudless day with 0.2. Therefore:

FO = (TOTRAD - AVRAD) / (TOTRAD - 0.2 * TOTRAD) (4)

Where,

TOTRAD is the total radiation completely cloudless day (J m -2 d -1, Table 1)

AVRAD is the true total incident radiation (J m -2 d -1).

If leaf canopy isn't closed as in the initial stages and at the end of the biological cycle, it does not absorbs the incoming radiation, which results in a CO_2 assimilation sufficiently lower than that in the case of restricted leaf

canopy. This decrease is approximated by the proportion of the incoming radiation absorbed from the culture (as discussed above) with the following relationship:

CFL = 1 - EXP (KE* LAI) (5)

Where,

CFL   is the percentage of theoretical radiation absorbed (0-1), and

KE   is the coefficient of permeation for visible light whose value ranges between 0.5 and 0.9 depending on the leaf geometry (Table.2).

The rate of CO_2 assimilation expressed in kg CO_2 ha -1 d -1. The absorbed CO_2 is reduced further to the culture in carbohydrates or sugars (CH_2O)n. To get assimilation rate expressed in carbohydrates, FGASS (kg (CH_2O) ha -1 d -1) then the rate of assimilation CO_2 (FGC) to should be multiplied by the ratio of molecular weights of carbohydrates and carbon dioxide(= 30/44) and on the weightings for temperature, the pervasiveness canopy leaf area and moisture availability:

FGASS = 30/44 * FGC * CFL * CFT * CFW (6)

Where,

FGASS is the total assimilation rate (kg (CH_2O) ha -1 d -1),
FGC is the total rate of assimilation leaf canopy (kg (CO_2) ha -1 d -1),
CFL is the radiation absorption coefficient (equation 5)
CFW is the water availability coefficient (= 1 when calculating potential output) (TRa/TRm)
CFT is the temperature coefficient (C-1) which is determined based on experimental data (field tests) or data from the literature (Driessen & Konijn, 1992, Van Heemst, 1988).

For the purposes of a simplified assessment, the CFT coefficient can be calculated from the relative decline of AMAX in Figure 1 assuming maximum civilian = 86 kg ha -1 h -1 for C 4-type plants and AMAX = 50 kg ha -1 h -1 for plants formula C 3.
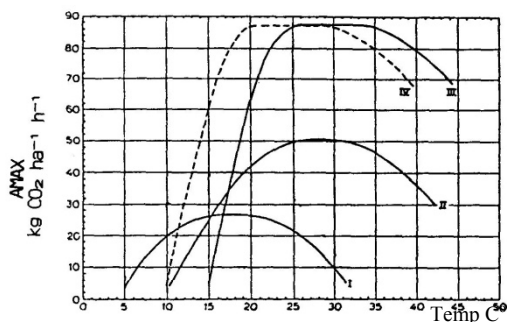
Figure 1. General AMAX reaction curves in temperature for different groups of crops (Versteeg & van Keulen, 1986). I = C3 plants in cold and temperate climates, II = C3 plants in hot climates, III = C4 plants in warm climates, IV = C4 plants in cold climates.

Furthermore, using table 2, we can predict the total growth rate of the crop dry mass (DWI) or the individual for Stem, Leaf, Root and Storage organs, combining the equations:

DWI = EC * (FGASS - MRR * TLDW) kg ha-1 d-1 (7)

Where,

DWI is the growth rate of the crop dry mass (kg ha-1),
EC is the conversion of carbohydrates into structural dry matter (average plant) (kg kg-1),
FGASS is the total rate of assimilation of the culture expressed carbohydrate (kg ha-1 d-1),
MRR is the relative rate of Maintenance respiration (total for all plant organs) (kg ha-1 d-1),
TLDW is the total dry weight of the (live) components of the culture (kg ha-1).

Therefore: DWI = FGC * (30/44) * CFT * CFW * 0.6 kg ha-1 d-1 (8)
Where,

0.6 is the Corrected: Growth respiration & Maintenance respiration

Spatial model calculation translation. Gathering the unknown factors from the previous equations we will try to convert them to surface models and feed them to a Raster Calculator based routine for further analysis. From Table 3, we can obtain the current unknown values that feeds the DWI model, as well as the transformations, the enhancements and the new sources for our GIS routine. On the next chapter we represent, the corresponding sensor needed for each acquisition and onboard or ground translation.

Table 3. Unknown values for model based DWI calculation, Translation methods, feeds and enhancements

Unknoun values	Units	Source	New Source	Variable	Shape Type	Tranlsation	New Shape Type
Crop							
Tbase	Celsius degrees	Litterature/lab	N/A	Model Parameter	Point	Equation Param.	within Raster calculator
Tsum1	Celsius degrees	Litterature/lab	N/A	Model Parameter	Point	Equation Param.	within Raster calculator
Tsum2	Celsius degrees	Litterature/lab	N/A	Model Parameter	Point	Equation Param.	within Raster calculator
Tref	Celsius degrees	Litterature/lab	N/A	Model Parameter	Point	Equation Param.	within Raster calculator
SLA	m^2 / kg	Litterature/lab	N/A	Model Parameter	Point	Equation Param.	within Raster calculator
KE	Factor	Litterature/lab	N/A	Model Parameter	Point	Equation Param.	within Raster calculator
LAI	m^2 /m2	Empirical/ Calculalted	Remote sensing	calculated Model Parameter	N/A	Equation	within Raster calculator
CFL	Percentage	Calculated	N/A	calculated Model Parameter	N/A	Equation	within Raster calculator
Environment							
Day Tmax	Celsius degrees	Weather station	N/A	Model Parameter	Point	Equation Param.	within Raster calculator
Day Tmin	Celsius degrees	Weather station	N/A	Model Parameter	Point	Equation Param.	within Raster calculator
Day Ta	Celsius degrees	Calculated	calculated(height interp. enhanced)	Model Parameter	Point	Krigging	Raster Surface
Day length N	hours	Literature Tables	calculated thru Solar radiation tool	Model Parameter	Point	Equation Param.	within Raster calculator
Day length n	hours	Literature Tables	calculated thru Solar radiation tool (slope enhanced)	Model Parameter	Point	Equation Param.	within Raster calculator
Day length N/n	Factor	Calculated	Calculated	Model Parameter	Point	Equation Param.	within Raster calculator
FCL	CO_2 (kg ha^{-1} d^{-1})	Literature Tables	Calculated (slope enhanced)	Model Parameter	Point	Equation P./Krigging	Raster Surface
FOV	CO_2 (kg ha^{-1} d^{-1})	Literature Tables	Calculated (slope enhanced)	Model Parameter	Point	Equation P./Krigging	Raster Surface
CFW	Percentage	Irrigation method	irrigation-evaportraspiration enhanced/Remote sensing	Model Parameter	Point	Equation/Krigging	Raster Surface
Derivatives							
CFTR	Factor			Calculated value	Point	Equation Param.	within Raster calculator
Tact	^{o}C-d			Calculated value	Point	Equation Param.	within Raster calculator
DVS	Percentage			Calculated value	Point	Equation Param.	within Raster calculator
FGC	kg ha^{-1} d^{-1}			Calculated value	Point	Equation Param.	within Raster calculator
FGASS	kg (CH_2O) ha^{-1} d^{-1}			Calculated value	Point	Equation/Krigging	Raster Surface

Building the platform

Materials. The complete list of materials used for the UAS platform is :

Navigation: Sensors needed for navigational algorithms, as well as extracting the orientation of captured images.
Autopilot AHRS   Ardupilot Mega 2.5
          Internal sensors:

Includes 3-axis gyro, accelerometer and magnetometer, along with a high-performance barometer.
Digital compass HMC5883L-TR chip.
Invensense 6 DoF Accelerometer/Gyro MPU-6000.
Barometric pressure sensor MS5611-01BA03.
Atmel's ATMEGA2560 and ATMEGA32U-2 chips for processing and usb functions respectively.

          External sensors:: Sensors needed for navigational algorithms, as well as extracting the position and exposure of captured images.
          GPS   ublox LEA-6H module.
          Airspeed sensor   MPXV7002 series piezoresistive transducer.
          Voltage and Current   AttoPilot Voltage and Current Sense Breakout - 90A.
          Luminance and Light   Adapfruit TSL2561 luminosity sensor.
Telemetry and Command   RFD900 1W transceiver at both sides with 3dbi Rubber duck antennas.

Remote Control
Transmitter   2,4Ghz Futaba 8FG(s)
Receiver   2,4Ghz Futaba R6008HS

Image Transmission: Real time image transmitters, feed our ground station with imagery, reducing time from acquisition to calculations.
Transmitter   5,8Ghz Foxtech 400mw with 1.25dbi Cloverleaf antenna
Receiver   5,8Ghz Foxtech RC805 with 12dbi Patch antenna

Payload Cameras: Low cost modified, Cameras needed to extract NDVI and point cloud models, for LAI estimation.
Visual Light   Canon sd780is point & shoot compact camera.
NIR modified   XNiteCanonELPH300NDVI point & shoot compact camera
Aircraft
          Parts
                    Fuselage   Phoreas model, Aramid-Carbon fiber epoxy resin laminated
                    Tail sector   CNC cut Styrofoam Core Cross Tail with All moving Stabilator
                          Airfoil naca 0012
                    Main Wings   CNC cut Styrofoam Core, polyvinyl sheeted with carbon fiber
          reinforcements
                          Airfoil naca 4412 (Skiptrovamon version)
                    Motor   Brushless Outrunner AC electric motor in pusher configuration
                    Battery   Three (3) cell Lithium polymer 11.1v 5000mah 35c Battery
                    Surface Movement Digital PWM driven servo motors
          Dimensions
                    Wing Span   2 m
                    Length   1.4 m
                    Wing Area   60dm^2
                    Weight (incl. payloads) 2400gr
                    Moving Surfaces   Ailerons, Elevator, Rudder, Flaps

Ground Station
          Laptop
                    Screen   15.6" LED type 1366 x 768, 16:9
                    Graphics   Intel HD Graphics 3000
                    Processor   Intel Core i5, 2450M
                    Memory   4 GB Memory Type DDR3
                    Hard Drive   320 GB SATA 3

Operating system	Microsoft windows 7, 64bit, Premium Edition
Software	ESRI ArcGIS 9.3, Michael Oborne's Mission Planner, VideoLan VLC media player, Autodesk Autocad 2010 lt
Image Capture	EZCap USB 2.0 Video/Audio Capture device
Internet connection	3G Broadband connection
External imagery resources	Hellenic Cadastral agency hi-resolution WMS service, USGS imagery and elevation data

Methods. Within years of aviation and remote controlled model aircraft, designers, manufacturers and Hobbyists, have pushed the limits of efficiency and material usage. Of the self products, have now days taken the roll of unmanned platforms for recreational purposes and remote sensing. Combining this knowledge with the specific needs of remote sensing, mapping and limiting factors such as Legislation, Terrain particularities, Payload capabilities, Payload size and production cost. Therefore we designed an aerial platform from the inside out, to fit our needs.

In order to test the platform we performed hundreds Simulation flights, testing the different wing shape type and airfoil, propulsion systems and materials. The flight envelop should fulfill the following requirements:

Maximum wingspan	2.4m, for easy transportation and deployment
Stall Speed	28km/h, For security purposes and maneuverability
Cruise Speed	35Km/h, for optimum image acquisition
Maximum airspeed	90 Km/h, for gusty wind penetration
Flight Duration	1 hour, for forest and sea mapping applications
Total weight	under 3kg, for legislation purposes and easy transportation and deployment
Payload capacity	1kg, to integrate a compact camera, autopilot, external sensors and aviation transponder

For our test we used XFLR5 windows software, which is an analysis tool for airfoils, wings and planes operating at low Reynolds Numbers and includes:
XFoil's Direct and Inverse analysis capabilities, wing design and analysis capabilities based on the Lifting Line Theory, on the Vortex Lattice Method, and on a 3D Panel Method.

Analysis results helped us conclude to the final design, which further tested on field for more than hundred (100) Hours, with onboard logging.

RESULTS

DWI translation Surface models

We selected a common corn crop productive county as the study area, where we had a great amount of field tests for DWI estimation from references, to test the liability of our GIS system. In table 4 we attach, the DWI estimations, calculated by the original model described on model translation methods, which have been verified by field tests.

Table 4. Field test samples and calculated values of DWI, for corn crop, from May to August in county Larissa, Greece (39o30')(source Danalatos et al., 2004)

Month	n/N	FCL	FOV	FGC	FGASS	DWI
May	0.611	843	354	652	445	266
June	0.656	892	388	712	485	291
July	0.744	873	368	744	507	304
August	0.760	788	329	678	462	277
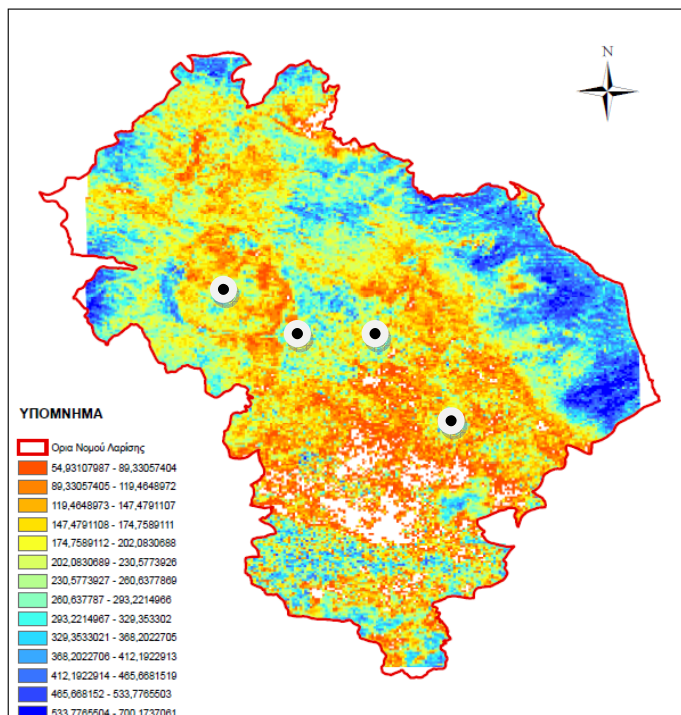
Figure 2. Example calculation of DWI for corn crop, at June in county Larissa, Greece, assuming total loss of breathing of 40% and natural (rain) irrigation, with spatial mapping. The field test values (Table 4)are marked with dots.

From the results summarized in Table 4 and figure 2 we see that the corresponding translation of the model routine in GIS predominates, since:

• It accurately calculates the incident radiation and latent one with the required pixel size derived scale, as well it considers the study area slope to the estimates.
• Results obtained in map form (Figure 2), planting link or a Cartesian coordinate system, make it easier to interpret. Therefore, producing the results from point-level (Table4), to surface analysis, makes possible multiple study area calculations at a time.
• Climate data determination was not done using statistics, or fed as such in our model, unlike the existing methods, the climatic conditions were determined separately for each cell with the Kriging method, minimizing the deviation.
• As shown in Figure 2, our system excluded from the map the non-agricultural land, subtracting from the results all areas with vegetation index near zero. Additionally, using influence and exclusion rules we can exploit the GIS multi-criteria analysis capabilities at the results and reverse lookup for cultivation area suggestions.

UAS remote sensing platform

Figure 3. Phoreas-Skiptrovamon modification, 3d Modeled isometric view.

The constructed UAS, designed with the described method and materials, features a low cross section drag, low weight platform, which satisfies the requested flight envelop, as well as modular design for robustness and further modifications.
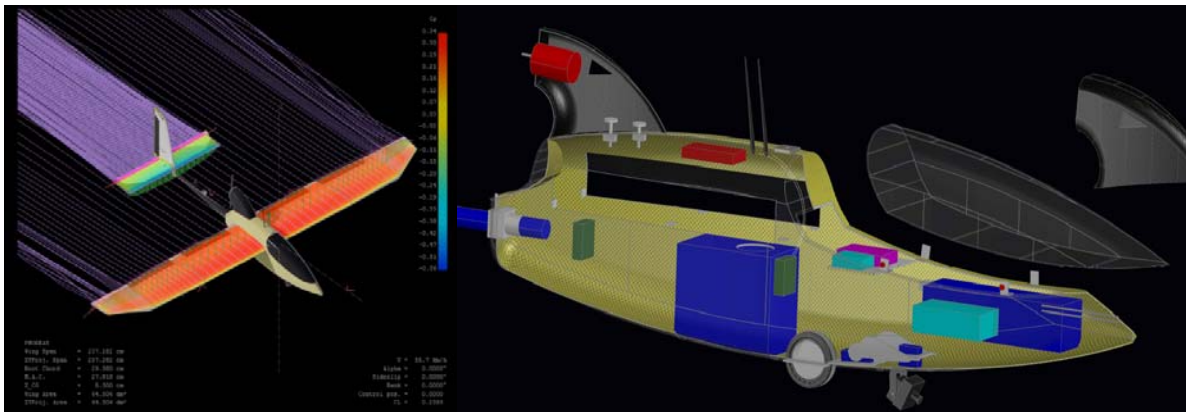
Figure 4. A. Caption from XFLR5 software, during the final stages of airfoil analysis. B.Caption from CAD Software, during gear in-fuselage arrangement. From left to right: Electric motor, Video transmitter module, ESC, Mapping camera case, Telemetry module, Autopilot, Remote control Rx, PTZ camera, Batteries.
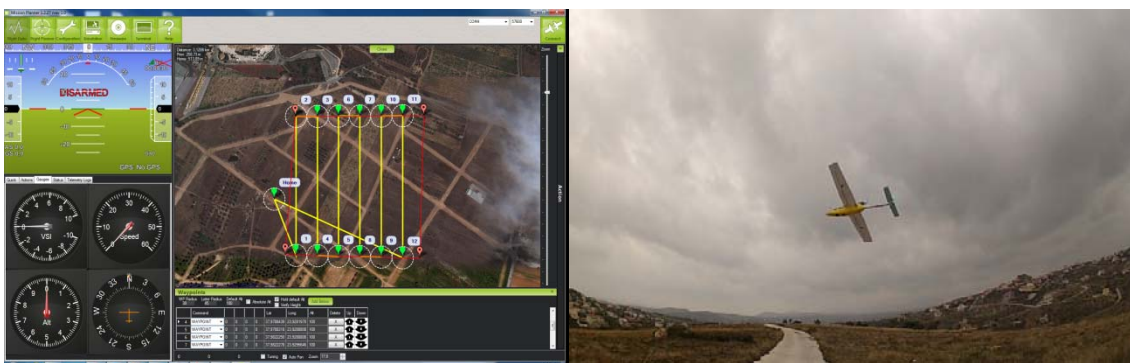
Figure 5. A.Screenshot Caption, from the Ground Control Station, during the lawnmower mission planning process (captured area ~5 acres, leg distance 60m, overlap 60%, flight Altitude 100m, travel distance 3,5km, mission time less than 10 min).B. UAS Performing near stall speed-low altitude maneuvers, during mapping tests, with 30km/h wind gusts.
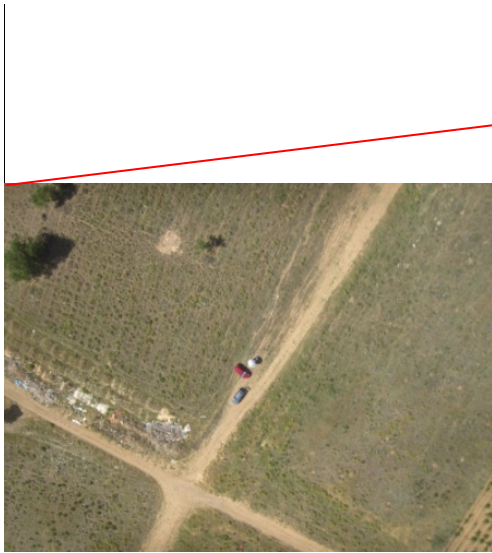
Image 2. Single unprocessed shot, from the mission, using Canon sd780is(focal length 5.9, Pixel width 4000, Pixel height 3000, ISO 400, Focus infinite, Shutter Speed
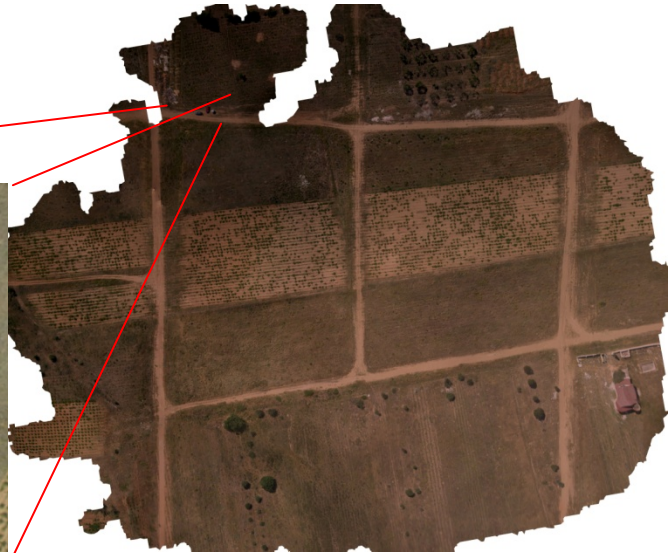
Image 3. Ortho Mosaic from 109 captions, Elevation model used has 4m intervals(source Hellenic Cadastral Agency), Ground resolution 2.57cm, 60% overlap 57% sidelap. (High resolution link, at references)

On image 2and 3 we present an example of a low cost image sensor. Like manned aerial imagery or satellite, all of them may record the reflection of the visible spectrum and the near infrared light, with 8-bit radiometric resolution. But spatial resolutions differs from 0,05m/cell to 0,5-30m/cell respectively. High resolution imagery, results on denser point cloud and accuracy which leads to better Canopy shape and size calculation to feed our routine. Also we have more detailed NDVI deviations for small foliages and plants like vineyards.
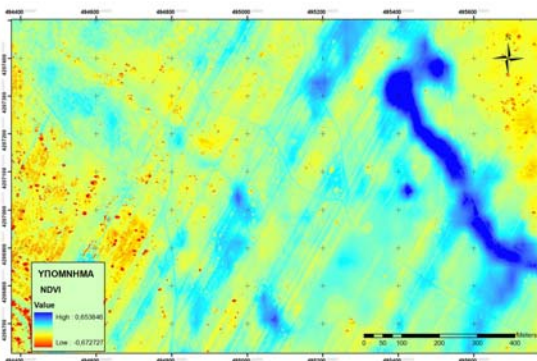
Figure 6 a. NDVI calculated from band 4-band 3 bands of UAS Ortho-mosaic (pixel size: 0.25 m)
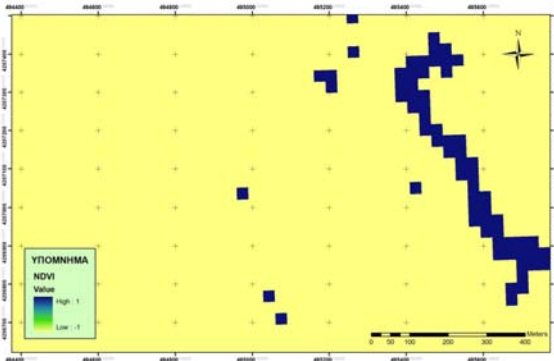
Figure 6 b. NDVI calculated from bands TM4-TM3 Landsat TM5 receiver (pixel size: 30m)

Unlike Satellite imagery, we can see that, the ortho georeferenced mosaic produced by the unmanned aircraft. With low altitude photography, did not exceed spatial resolution more than 0.25 m / cell, with capabilities up to 0.05 m / cell. The high spatial resolution combined with high radiometric capability given us the opportunity to have exact classification of the vegetation of the region, as shown by the respective (a,b) calculation of NDVI in Figure 6.

CONCLUSIONS

With continuous monitoring and modeling, we have the ability to reverse the over-fertilization for the benefit of existing crops in both qualitative upgrading of products (like wine) and quantitative (Like biofuels and Cattle feeds). This will provide the opportunity for farmers to use every resource available and to return to active production without the need for subsidies and effect in accordance with the latest certification standards.

Increasingly, we are experiencing the need for lower cost produced information. The flight costs are minimal and all it requires is the physical presence of the aircraft, as opposed to aerial photography from manned aircraft. Compared with the satellite images, the image produced has much higher resolution (0,05m/cell to 0,5-30m/cell respectively) without the overcast obstructions and can be repeated at any time.

Using open source software and avoiding expensive software in most steps of the recording and processing of data (aircraft, ground station, post-processing), keeps the operating costs low, while involves rapidly thanks to the growing community, of active end users and developers.

REFERENCES

Almhab, A., Busu, I., 2008, "Estimation of Evapotranspiration with Modified SEBAL Model Using Landsat-TM and NOAA-AVHRR Images in Arid Mountains Area", Modeling & Simulation, 2008. AICMS 08. Second Asia International Conference, 350 – 355

C.T. de Wit, 1968, "Plant Production" Kluwer Academic, Netherlands

Danalatos N.G. , Archontoulis S.V, 2004, "Potential growth and biomass productivity of kenaf (hibiscus cannabinus l.) under central greek conditions: ii. the influence of variety, sowing time and plant density, 2nd World Conference on Biomass for Energy, Industry and Climate Protection, Rome, Italy

Duncan J. Acheson, 1967, "Quality Control and Industrial Statistics.", Richard D. Irwin Inc., Homewood, Illinois

Goudriaan J., 1977, "Crop micrometeorology: a simulation study. Simulation Monograph, Pudoc, Wageningen

Goudriaan J.,Van Laar, 1994, "Modeling potential crop growth processes: textbook with exercises", Kluwer Academic, Netherlands

Hatzopoulos J. N., 2008, "Topographic Mapping" Covering the wider field of Geospatial Information Science & Technology (GIS&T). Universal Publishers, 740 pages.

Nikos Andrulakakis, Ilias Kontakos, Kostis Koutsopoulos, 2010, Introduction to Geo-statistics, Advance GIS class, Seminar guide, University of Thessaly, National Technical University of Athens, School of Rural and Surveying Engineering, Athens

Herwitz S.R., et al, 2004, "Imaging from an unmanned aerial vehicle: agricultural surveillance and decision support", Computers and Electronics in Agriculture, Vol. 44, Issue 1, 49–61

Hideki Yoshimoto, Kazuhiro Jo, Koichi Hori, 2008, "Design of installation with interactive UAVs", CE '08 Proceedings of the 2008 International Conference on Advances in Computer Entertainment Technology

Johnson L.F., et al, 2001, "In-season prediction of potential grain yield in winter wheat using canopy reflectance." Agronomy journal. vol. 93 (1), 131-138.

Johnson L.F., et al, 2003, "Collection of Ultra High Spatial and Spectral Resolution Image Data over California Vineyards with a Small UAV", Proceedings, Int'l Symposium on Remote Sensing of Environment 2003

P. M. Driessen, N. T. Konijn, 1992, "Land-use systems analysis", Wageningen Agricultural University, Wageningen

Paul J Pinter, et al, 2003, "Remote Sensing for Crop Management", Photogrammetric Engineering Remote Sensing, vol. 69, issue 6, 647-664

Wit. C.T. De, F.W.T Penning de Vries, 1982, "l'analyse des systems de production primaire" In: F.W.T Penning de Vries, s.m.a. Djiteye, La productivite des paturayes suheliens. Pudoc, Wageningen

Xiaopeng Li, Jiabao Zhang, Jintao Liu, Jianli Liu, Anning Zhu, Fei Lv, Congzhi Zhang, 2011, "A modified checkbook irrigation method based on GIS-coupled model for regional irrigation scheduling", IRRIGATION SCIENCE, Vol. 29, 2, 115-126

http://api.ning.com/files/ngAjojnN4tc4-oDE4HcviQFU9WRYt7yWWjAr1JPxDdpuA-XsUsqCjcVjBRCLcQbvy*tuXhtHvoxaVslLVA5cJw__/stiched_spata.jpg?transform=rotate(270)

ACKNOWLEDGMENTS